RSC Pharmaceutics

ROYAL SOCIETY OF CHEMISTRY

PAPER

View Article Online
View Journal | View Issue

Cite this: *RSC Pharm.*, 2026, **3**, 150

Sustained drug delivery of the β-blocker acebutolol hydrochloride *via* chitosan–bilimbi leaf extract films

Jennifer P. Pinto, [a] Manjunath B. Megalamani, [b] Ajitkumar Appayya Hunashyal,[c] Oshin Jacintha D'souza,[a] Sharanappa T. Nandibewoor, [d] Saraswati P. Masti [c] and Ravindra B. Chougale *[a]

This study presents the development of biocompatible polymeric films designed for the sustained release of the β-blocker acebutolol hydrochloride (AH). The films were fabricated using chitosan (CH), a biodegradable biopolymer, in combination with varying concentrations of *Averrhoa bilimbi* leaf extract (ABE), a natural additive with potential antimicrobial properties. The composite films were characterized using crystallinity, spectroscopic, mechanical, thermal, and morphological analyses. Functional testing included swelling studies, cumulative drug release profiling, cytotoxicity assessments, and microbial resistance assessments. The results indicated that the incorporation of ABE positively influenced the structural, mechanical, thermal and morphological properties, including swelling behaviour, thickness, and drug release kinetics. The film with the lowest ABE concentration showed optimal swelling (~200%) and the highest drug release (~25%), along with notable drug loading (~78%) and encapsulation efficiency (~19%). The release kinetics followed the Higuchi and Korsmeyer–Peppas models, indicating a non-Fickian diffusion mechanism. Importantly, the AH integrity was maintained throughout the fabrication process, and all the films exhibited excellent biocompatibility (90% cell viability rate). These findings support the feasibility of using CH/ABE films as promising candidates for sustained drug delivery systems. The use of plant-based and biodegradable components underscores the potential of this green strategy in pharmaceutical formulations, contributing to sustainable chemistry and reducing the environmental impact in drug delivery applications.

Received 30th June 2025,
Accepted 8th October 2025

DOI: 10.1039/d5pm00172b

rsc.li/RSCPharma

1. Introduction

Engineering novel drug delivery systems (DDS) has become a focus in the field of pharmaceutical research. The therapeutic process of drug administration requires a competent drug delivery mechanism. The mechanism involves three major steps: administration of the drug, release of the active pharmaceutical ingredient, and transportation of the drug to its targeted site.[1] Drug delivery systems mainly emphasize liberating a particular drug at the appropriate time and concentration towards a specific target site.[2] It has been observed over the years that the conventional systems for drug delivery such as tablets, pills, syrups, injectables, *etc.*, have been facing issues of intermittent drug release profiles in addition to the scarcity of bioavailability of the drugs.[3] The major loophole of these traditional DDS is the lack of controlled release of the drug accompanied by irregular biodistribution at indefinite sites, resulting in detrimental effects on the health of individuals. To combat this issue, advanced systems of drug delivery that mitigate the controlled release of drugs have been developed. The foremost challenge of these advanced systems lies in limiting the dosage and sustaining the concentration of the drug at a particular location.[4]

The use of natural polymers in tailoring films apt for DDS has gained substantial attention from researchers over the past few decades. The prime rationale behind this could be their biocompatibility and defensive properties.[5] In addition, their drug-loading efficiency and ability to confirm controlled release of the drug over a constant time interval at definite proportions add to their advantages. For a polymer to act as a resourceful drug delivery vehicle, the main prerequisites are bioerodibility, bioresorbability and biodegradability.[6] Biopolymers such as chitosan, gelatin, pullulan, cellulose, carrageenan, *etc.*, meet these requisites and hence their pro-

[a]*P. G. Department of Studies in Chemistry, Karnatak University, Dharwad-580 003, India. E-mail: chougalerkud19@gmail.com*
[b]*Sustainable Energy and Nanomaterials Technology Research Applications Laboratory, Atria Institute of Technology, Bengaluru – 560024, India*
[c]*Department of Chemistry, Karnatak Science College, Dharwad-580 003, India*
[d]*Department of Chemistry, School of Advanced Sciences, KLE Technological University, Hubballi-580031, India*

perties have been effectively harnessed in the area of pharmaceutical research, particularly in DDS.[7–11]

Chitosan (CH) is one of the natural cationic polymers that has gained much recognition owing to the presence of functionally active groups in its structure which impart massive physicochemical properties. The inherent properties of chitosan such as reduced immunogenicity and toxicity, biodegradability, biocompatibility, and bacterial resistivity allow it to be highly utilised in the field of medicine as drug carriers, wound dressing agents and antibacterials.[12] Also the property of CH as a biocompatible and biodegradable polymer ensures its applicability in biomedical applications.[13] The abundance of free hydroxyl and amino groups in the structure of CH endows it with mucoadhesive properties since these groups favorably interact with mucosal tissues.[14] Barring all these advantages of CH, the property of high-water absorption[15] by CH along with its sparse mechanical properties hinders its application in controlled drug release technologies.[16] Hence, to tame these drawbacks, blending CH with suitable dopants, extracts or nanofillers is gaining prominence.

Averrhoa bilimbi (AB), commonly known as bilimbi, is a prominent plant found in the tropical and subtropical regions, known for the presence of high concentrations of several phytopharmaceuticals in it.[17] In a study reported by Valsan and Raphael describing the pharmacognostic profile of AB leaves, the presence of both primary and secondary metabolites such as carbohydrates, sugars, cardiac glycosides, flavonoids, phenols, saponins, *etc.*, was clearly observed. These potential compounds of pharmacological importance transmit antimicrobial, anticancer and antioxidant properties and are also known for their capacity to control blood cholesterol levels.[18] Thus, the medicinal importance of *Averrhoa bilimbi* leaves can be effectively utilized in DDS by blending its extract with CH.

Acebutolol hydrochloride (AH) is a cardioselective beta-blocker drug primarily used in treating cardiovascular ailments, particularly hypertension, angina and also thyrotoxicosis.[19,20] The pharmacokinetic parameter 'elimination half-life ($T_{1/2}$)' of a drug is the time taken for a particular drug to reduce to 50% of its concentration in the body.[21] It is found that the $T_{1/2}$ of AH is nearly 3–4 h in plasma and 8–13 h in the case of its metabolite, diacetolol.[22] Notably, it can be inferred that AH can be released into the body at a controlled rate *via* drug-delivering films, rather than by intravenous administration.

A wide range of research has been carried out on CH films employed as DDS. Affes *et al.* developed CH films loaded with ciprofloxacin and studied the release behavior of the drug, which proved that CH possessed the ability to release the drug sustainably.[7] Barman *et al.* reported that CH films reinforced natural halloysite nanotubes containing norfloxacin as potential drug delivery vehicles providing enhanced therapeutic benefits.[23] Divya Radha, Jisha S. Lal and K. S. Devaky studied the release profile of the anticancer drug 5-fluorouracil from chitosan and banana peel extract.[6] However, the use of a cardioselective β-blocker in combination with CH and a leaf extract, which in this case is ABE, has not been previously reported.

The major aim of controlled release drug delivery is to avoid the frequent administration of dosages. Drugs such as AH have relatively short half-lives, which necessitate the requirement of a sustained release system. Therefore, an effective and controlled release drug-delivery system evades the requirement of frequent dosage. Hence, the fabrication of a controlled-release system in the form of a flexible film with CH as the host matrix was chosen. Since CH films have limitations of brittleness and water absorption, they are inhibited by the addition of bioactive constituents such as plant extract, which in this case is ABE. ABE possesses useful phytochemical components that enhance the therapeutic efficiency of the films. The present work aims to fill the research gap of incorporating a β-blocker drug into a plant extract mediated polysaccharide film.

The hypothesis of this study was to examine the effect of AB extract on CH films in enhancing their physicochemical, morphological, and biological properties to develop a biocompatible and sustainable channel for the controlled release of AH. Accordingly, this work focused on creating films using CH and the drug AH with increasing concentrations of AB extract. The release of AH by the incorporation of AB extract and its subsequent addition in increasing concentrations to the CH matrix was studied for understanding swelling, drug loading efficiency and encapsulation, and release kinetics along with the films' biocompatibility and microbial resistance.

2. Materials and methods

2.1 Chemicals used

Chitosan (viscosity: 5–20 mPa s, molecular weight: 1526.464 g mol^{-1} and deacetylation degree: 70%) was obtained from Tokyo Chemical Industry (TCI), Japan. Acebutolol hydrochloride ($C_{18}H_{28}N_2O_4$·HCl, molecular weight: 372.89 g mol^{-1}) was procured from Sigma Aldrich. Phosphate buffered saline (PBS) (pH: 7.4 ± 0.1) was purchased from Sisco Research Laboratories (SRL) Pvt. Ltd India. Acetic acid (glacial) ($C_2H_4O_2$, molecular weight: 60.05 g mol^{-1}) was obtained from SD Fine Chemicals, India. *Averrhoa bilimbi* leaves were obtained from the local areas of Dharwad, Karnataka, India. The plasticizer glycerol ($C_3H_8O_3$, molecular weight: 92.09 g mol^{-1}) was obtained from Loba Chemie Pvt. Ltd. All chemicals used in this study were of purely analytical grade and millipore water was used throughout this work.

2.2 Preparation of *Averrhoa bilimbi* leaf extract (ABE)

Averrhoa bilimbi leaves were washed thoroughly with water and dried under shade for about a week. The dried leaves were ground using a blender and the powder was collected. 10 g of this dried leaf powder were accurately weighed and soaked in a 1 : 1 solution of ethanol and water. The solution containing the soaked leaves was macerated for three days. The solution was filtered using Whatman filter paper no. 41 and the filtrate was collected and stored at 4 °C until further use. This extract was analyzed for its phytochemicals by measuring the total

phenolic content (TPC) and analyzing it with gas chromatography–mass spectrometry (GC-MS) for a detailed overview.

2.3 Preparation of acebutolol hydrochloride (AH) drug-loaded chitosan (CH)/*Averrhoa bilimbi* leaf extract (ABE) films

The films designed for drug release were obtained by applying the solvent casting technique. The compositions of the films are listed in Table 1. CH (0.5 g) was weighed and dissolved in 50 mL of 1% glacial acetic acid solution. This solution was magnetically stirred. The ABE was added to the CH solution at varying concentrations slowly to ensure a homogeneous solution. The AH drug (20 mg) was added to this composite solution by dissolving it in 5 mL of water. 1% glycerol (1 mL) was added to the solution. The composite solution was stirred for about three hours and then finally cast onto glass petri plates. The solvents were allowed to evaporate, and the dried films so obtained were peeled from the petri plates and stored in a desiccator until further investigation. Fig. 1 shows images of the fabricated films.

3. Characterisation techniques

3.1 Phytochemical characterisation of the *Averrhoa bilimbi* leaf extract (ABE)

3.1.1 Total phenolic content (TPC) of the ABE. The analysis of the phenolic compounds in the ABE was conducted using a well-known method called the Folin–Ciocalteu (F–C) method.[24] Accordingly, 0.5 mL of the ABE solution was mixed with 1 mL of the FC reagent and allowed to incubate for about 6 minutes. After this, approximately 3 mL of 8% sodium carbonate (Na_2CO_3) was added to the mixture, which was then incubated for an additional half an hour. The absorbance of this solution was measured at 765 nm, indicating the concentration of phenolics in the ABE. A calibration curve using gallic acid was plotted following the same procedure. The TPC of the ABE was expressed in GAE per mg.

3.1.2 Chemical composition of the ABE. The different chemical components present in the ABE were accurately evaluated using gas chromatography–mass spectrometry (GC-MS). The ABE sample was placed into the chamber of the Shimadzu GC-MS-QP2020, and the analysis was performed. The interpretation of the individual compounds was done using a NIST-23 mass spectral library.

Table 1 AH reinforcement in the CH/ABE composite films

Sample code	Chitosan (CH) (g)	*Averrhoa bilimbi* leaf extract (ABE) (mL)	Acebutolol hydrochloride (AH) (g)
CD	0.5	—	0.02
CAD-1	0.5	1.0	0.02
CAD-2	0.5	2.0	0.02
CAD-3	0.5	3.0	0.02

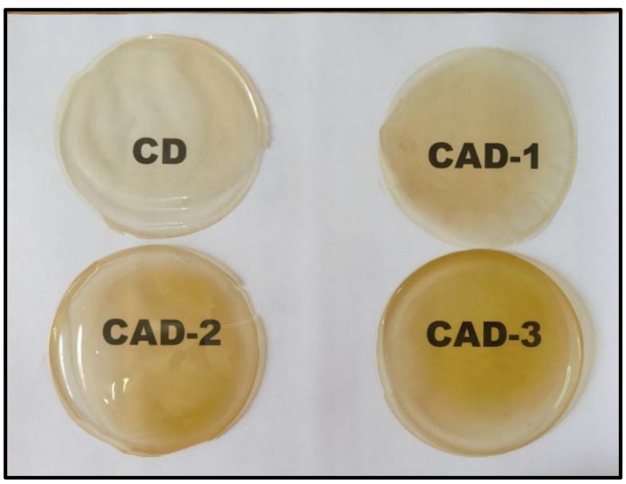

Fig. 1 Images of the developed films.

3.2 Characterisation of the CH/ABE/AH films

3.2.1 Measurement of crystallinity. To investigate the crystallinity of the developed films, X-ray diffraction (XRD) analysis was performed. The film samples were cut into 1 × 1 cm^2 pieces and inserted into the sample holder of a SmartLab SE (Japan) X-ray diffractometer. The analysis was carried out using a Cu-κ_β source and the diffraction peaks were obtained in the 2θ range of 5–80° with a scan rate of 5° min^{-1}. The crystallinity percentage of the films was evaluated using the following relation (1):[25]

$$\text{Crystallinity percentage}\ (\%) = \frac{A_c}{A_0} \times 100 \qquad (1)$$

where A_c and A_0 correspond to the total area of the crystalline peaks and the total area of all peaks observed in the diffractograms, respectively.

3.2.2 Spectroscopic analysis. The changes occurring between the components of the composite films were effectively recorded using attenuated total reflectance–Fourier transform infrared spectroscopy (ATR–FTIR). The analysis of the films was carried out over the wavenumber range of 400–4000 cm^{-1} using a Nicolet IN-10 High-resolution FTIR spectrometer at ambient temperature.

3.2.3 Measurement of thickness and mechanical properties. The thickness of the fabricated films was measured using a micrometer (Mitutoyo Digital Micrometer, Japan) at four random locations on the film. The average thickness of the films was reported. The mechanical properties of the films were tested on a Universal Testing Machine (DAK System, Mumbai) by fixing a film sample of dimensions 10 × 2.5 cm^2 into the extension grip of the instrument with a grip distance of 5 cm initially. The films were stretched at a crosshead speed of 1 mm min^{-1}.

3.2.4 Thermal analysis. To study the thermal stability of the films, differential scanning calorimetry (DSC) analysis was carried out. The film samples were placed in an aluminium crucible in an inert gas (nitrogen) atmosphere in a Setaram KEP Technologies SETLINE DSC/SA instrument. The tempera-

ture range of analysis was room temperature up to 400 °C at a 10 °C min^{-1} heating rate.

The percentage of crystallinity was also calculated using the data from the thermograms such as ΔH_f (the enthalpy of fusion of the film at the melting temperature) and ΔH_{f100} (the enthalpy of fusion of the 100% crystalline chitosan, *i.e.* 62.05 J g^{-1}). These were subsequently used in the following eqn (2):[26]

$$\text{Crystallinity percentage}\,(\%) = \frac{\Delta H_f}{\Delta H_{f100}} \times 100 \quad (2)$$

3.2.5 Morphological analysis. To obtain a better understanding of the surface morphology of the developed films, they were subjected to scanning electron microscopy (SEM) imaging. Priorly gold sputter-coated film samples of dimensions 1 × 1 cm^2 were adhered onto the sample holder of the JEOL-JSMIT500LA instrument. The images were recorded at an accelerating voltage of 5 kV.

3.2.6 Hydrophobicity measurements. To examine the surface wettability property of the films, a 2 μL water droplet was made incident on film samples of dimensions 2 × 2 cm^2 using a microsyringe. The water contact angle was measured through the Kyowa Interface Science DMS-401 analyser by using the sessile drop technique. The image of the droplet on the surface of the film was captured using a high-resolution camera.

3.2.7 Swelling studies. The AH drug-loaded films were studied for their capacity to swell in the desired solution. Priorly weighed film samples of dimensions 1 × 1 cm^2 were immersed in 10 mL of phosphate-buffered saline (PBS) solution of pH 7.4. The swollen films were withdrawn from the solution at regular intervals of time, followed by blotting with filter paper, and then accurately weighed. The percentage of swelling of these films was measured using eqn (3):[27]

$$\text{Percentage of swelling} = \frac{W_{st} - W_i}{W_i} \times 100 \quad (3)$$

where W_{st} and W_i correspond to the weight of the swollen film at time '*t*' and the initial weight of the film sample, respectively.

3.2.8 *In vitro* release studies. The calibration curve for the absorbance of the AH drug was plotted using the serial dilution method. AH (1 mg) was dissolved in 100 mL of water to form a stock solution. 0.2 mL, 0.4 mL, 0.6 mL, 0.8 mL and 1 mL were extracted from this stock solution and diluted to 10 mL in a volumetric flask. The resulting concentrations of the solutions were found to be 2, 4, 6, 8 and 10 μg mL^{-1}. The maximum absorbance values of these solutions were recorded at 232 nm and a calibration curve was plotted. The drug release study was carried out according to the method reported by Radha, Lal and Devaky with few modifications.[6] The AH-reinforced films of dimensions 1 cm × 1 cm were sealed in a dialysis membrane containing 2 mL of buffer solution. This dialysis bag was sunk in 100 mL of phosphate buffered saline (PBS) release medium of pH 7.4 and allowed to stir at 37 °C. 5 mL of this solution was drawn at definite time intervals. The overall volume of the release medium was maintained constant by adding 5 mL of PBS each time the solution was withdrawn. The absorbance values of the withdrawn samples were analyzed at 232 nm, and the concentration of the drug released was determined using the calibration curve.

3.2.9 Drug loading efficiency. The capacity of the film to maintain a certain drug concentration was examined using UV–visible spectrophotometry. Priorly weighed AH-loaded films (W_i) were swollen in 30 mL of PBS solution. The solutions containing these films were then agitated at a high speed for about 45 min to ensure complete and paced release of the drug in the release medium. The solution was then filtered and subjected to UV–visible spectroscopy at a wavelength of 232 nm and the consequent amount of drug present in the film (W_f) was determined. The percentage of drug loading and encapsulation efficiency were calculated using the following formulae (4) and (5)[28]

$$\text{Percentage of drug loading} = \frac{W_f - W_i}{W_i} \times 100 \quad (4)$$

$$\text{Encapsulation efficiency (EE)} = \frac{\text{Percentage of drug loading (actual)}}{\text{Percentage of drug loading (theoretical)}}. \quad (5)$$

3.2.10 Kinetics of drug release. The drug release kinetics was analysed from the drug release profile data and the results were incorporated into the mathematical equations of the zero order, first order, Higuchi and Korsmeyer–Peppas models. Eqn (6)–(9) represent the above-mentioned kinetic models:[29]

Zero order model:

$$M_t = K_t \quad (6)$$

First order model:

$$\log M_t = \frac{K}{2.303} t \quad (7)$$

Higuchi model:

$$M_t = K\sqrt{t} \quad (8)$$

Korsmeyer–Peppas model:

$$\log \frac{M_t}{M_\infty} = \log K + n \log t \quad (9)$$

Here, M_t represents the amount of drug (AH) released at time *t*. *K* and *n* correspond to the release rate constant and the release exponent, respectively, while M_∞ is the amount of drug present in the sample.

3.2.11 Cytotoxicity studies. The methyl thiazolyl tetrazolium (MTT) assay was used to study the cytotoxicity of the fabricated films. This analysis was carried out on L929 mouse skin fibroblast cell lines. According to this study, the viability of the cells was determined based on the reduction of mitochondrial dehydrogenase by MTT assay *via* the formation of an insoluble purple-coloured formazan salt. The intensity of the purple coloration corresponded to the number of viable cells, which was measured at an absorbance of 570 nm.[23] Using Dulbecco's modified Eagle medium (DMEM) supplemented

with 10% fetal bovine serum (FBS) and antibiotics such as streptomycin and penicillin, the cells were allowed to grow at 37 °C in an incubated carbon dioxide (5%) atmosphere for 24 h. Following this, the cell culture was washed with PBS and treated with MTT (200 μL). The entire mixture was further incubated for 3 h at 37 °C. The test was terminated by adding DMSO to the culture wells, and the amount of formazan formed was examined using a microplate reader to determine absorbance. The cell viability percentage was calculated using the formula given in eqn (10).[30]

$$\text{Cell viability}\,(\%) = \frac{\text{OD of test sample}}{\text{OD of control}} \times 100 \qquad (10)$$

3.2.12 Bacterial resistance. The antibacterial efficacy of the drug-loaded films was evaluated against Gram-positive bacteria *Staphylococcus aureus* (NCTC 10788) and Gram-negative bacteria *Escherichia coli* (ATCC 25922) by the disc-diffusion method according to a report by the National Committee for Clinical Laboratory Standard (NCCLS) with minor modifications.[31] On a sterile nutrient agar plate, 100 μL of the suspension of bacterial culture was swabbed. Film discs of 6 mm were placed on the petri plate and incubated at 37 °C for 24 h. The antimicrobial activity results were presented as the mean diameter of the inhibition zone in mm ± standard deviation (mean ± SD).

3.2.13 Statistical analysis. Origin-18 software was used for statistical analysis. One-way analysis of variance was employed. All tests so performed were carried out in triplicate and the results were presented as average values along with a standard deviation (n = 3) from an average value. To differentiate between the mean values, Tukey's test was used at a significance level of $p \leq 0.05$.

4. Results and discussion

4.1 Phytochemical analysis of the *Averrhoa bilimbi* leaf extract (ABE)

4.1.1 Total phenolic content of the ABE. The leaves of AB are prominent for their pharmacological activity owing to the presence of a wide variety of phytochemicals, which impart a wide spectrum of chemical and biological activities. The measure of the total phenolic content gives an overview of the quantity of plant polyphenols present in a given extract. The TPC of the ABE was found to be 108.84 GAE mg^{-1}, which apparently confirmed the presence of polyphenolic compounds. This value was in agreement with that reported by previous research.[32]

4.1.2 Chemical composition of the ABE. The leaves of AB are widely recognized for their medicinal properties due to the existence of bioactive compounds. Fig. 2 and Table 2 offer a summary of the bioactive compounds identified in the ABE through the GC-MS technique. The leaves of *Averrhoa bilimbi* are well known for their pharmacological relevance, which is supported by the presence of phytochemicals detected using the GC-MS technique. The data revealed the presence of terpenes such as phytol, neophytadiene, squalene, and β-amyrin which are reported to inhibit inflammation, microbial attack, oxidation, cancer *etc*. In addition to these properties, these compounds are also known to impart anxiolytic and anticonvulsant effects, enhancing the role of the CAD films as β-blockers.[33–36] Also, the presence of phytosterols such as stigmasterol, sitosterol, stigmastanol, and sitostenone, all of which exhibit medicinal activity, prominently helps in lowering cholesterol levels in humans.[37–39] Vitamin E has also been detected in the ABE. The presence of these phytochemicals helps elevate the functionality of the CAD films as drug-delivering films.

4.2 Analysis of the properties of the CH/ABE/AH films

4.2.1 Percentage of crystallinity. The films were analysed for their crystallinity percentages. Fig. 3[A] displays the X-ray diffractograms of the AH-loaded films and Table 3 indicates the crystallinity percentages of the developed films. AH is found to be highly crystalline in nature.[40] However, when this drug was incorporated into the film matrix, the crystallinity of AH was not evident in the diffractograms. This readily stipulates that AH was dispersed uniformly in the CH matrix, leading to the absence of any additional peaks in the obtained diffractograms.[41] From the observations drawn, it is evident that the broad peak at around 22.5° corresponds to the semi-crystalline nature of CH.[25] There was no significant difference observed between the diffractograms of the CD film and the films containing ABE, indicating that the AB extract was blended effectively and was distributed uniformly within the CH matrix. In accordance with this, it was also noticed that

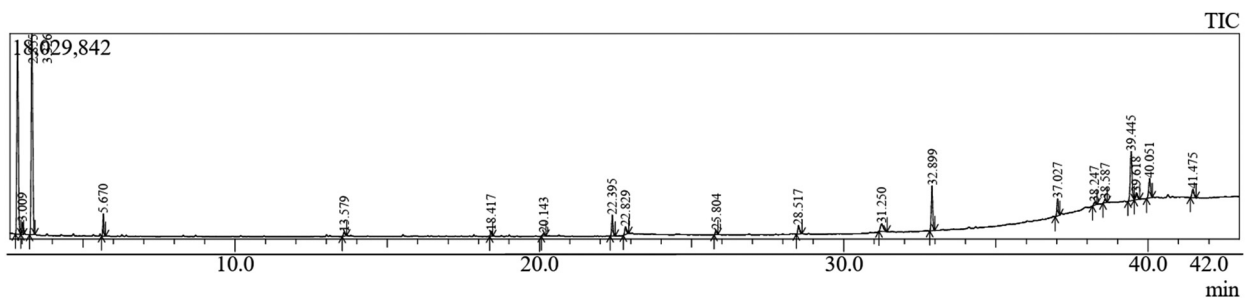

Fig. 2 GC-MS profile of *Averrhoa bilimbi* leaf extract.

Table 2 Chemical constituents detected by GC-MS analysis of the ABE

Peak #	Retention time	Area (%)	Name	Structure
1	2.855	29.35	Ethane, 1,1-diethoxy-	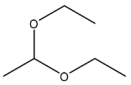
2	3.009	1.47	1-Butanol, 3-methyl-	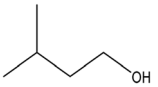
3	3.326	30.38	Propane, 2,2-diethoxy-	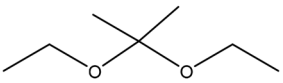
4	5.670	2.41	Ethyl 4-(ethyloxy)-2-oxobut-3-enoate	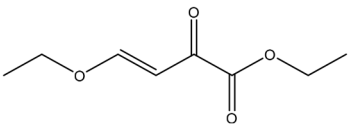
5	13.579	0.64	1,3-Propanediol, 2-(hydroxymethylyl)-2-nitro	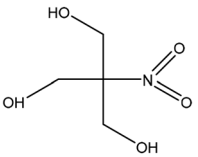
6	18.417	0.57	Neophytadiene	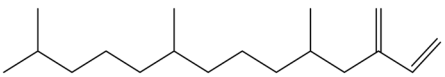
7	20.143	0.46	*n*-Hexadecanoic acid	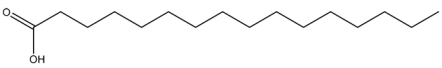
8	22.395	2.83	Phytol	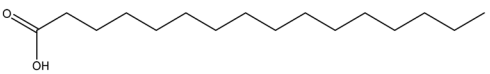
9	22.829	1.34	9,12,15-Octadecatrienoic acid, (*Z*,*Z*,*Z*)-	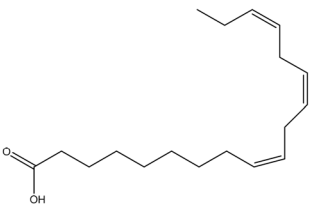
10	25.804	28.517	9,12,15-Octadecatrienoic acid, ethyl ester, (*Z*,*Z*,*Z*)-	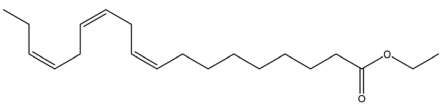
11	28.517	1.52	Benzyldiethyl-(2,6-xylylcarbamoylmethyl)-ammonium benzo-	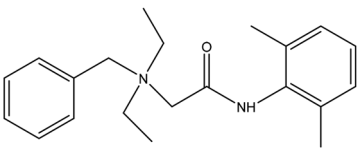
12	31.250	2.19	9,12,15-Octadecatrienoic acid, 2,3-dihydroxypropyl ester, (Z,Z,Z)	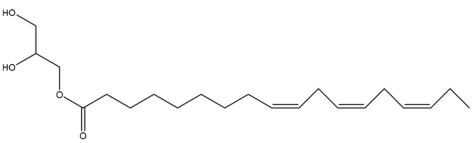
13	32.899	6.46	Squalene	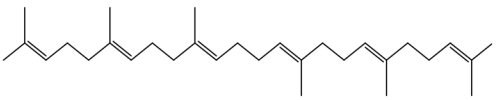
14	37.027	2.55	Vitamin E	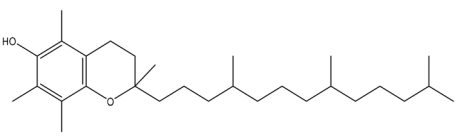

Table 2 *(Contd.)*

Peak #	Retention time	Area (%)	Name	Structure
15	38.247	0.57	Ergost-5-en-3-ol, (3.beta.)-	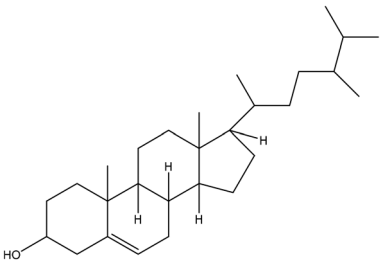
16	38.587	0.58	Stigmasterol	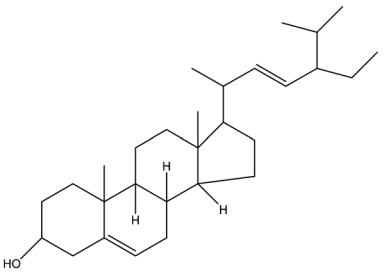
17	39.445	9.24	γ-Sitosterol	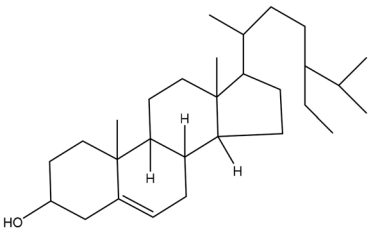
18	39.618	1.45	Stigmastanol	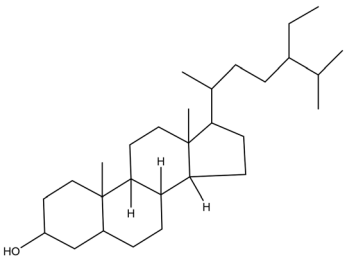
19	40.051	3.63	β-Amyrin	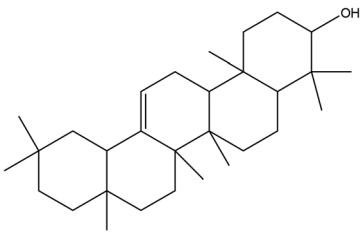
20	41.475	1.71	γ-Sitostenone	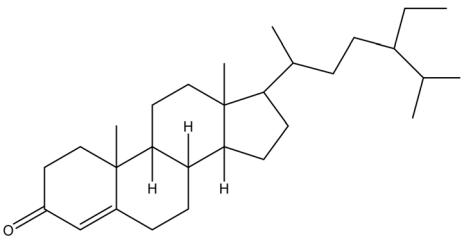

the crystallinity percentages of the fabricated films increased with the reinforcement of higher concentrations of ABE. ABE possesses a wide range of functional groups such as polyphenols, carboxylic acids, and hydroxyl groups which are abundant in polar groups. These groups assist in the formation of strong hydrogen bonds with the polysaccharide matrix used,[42]

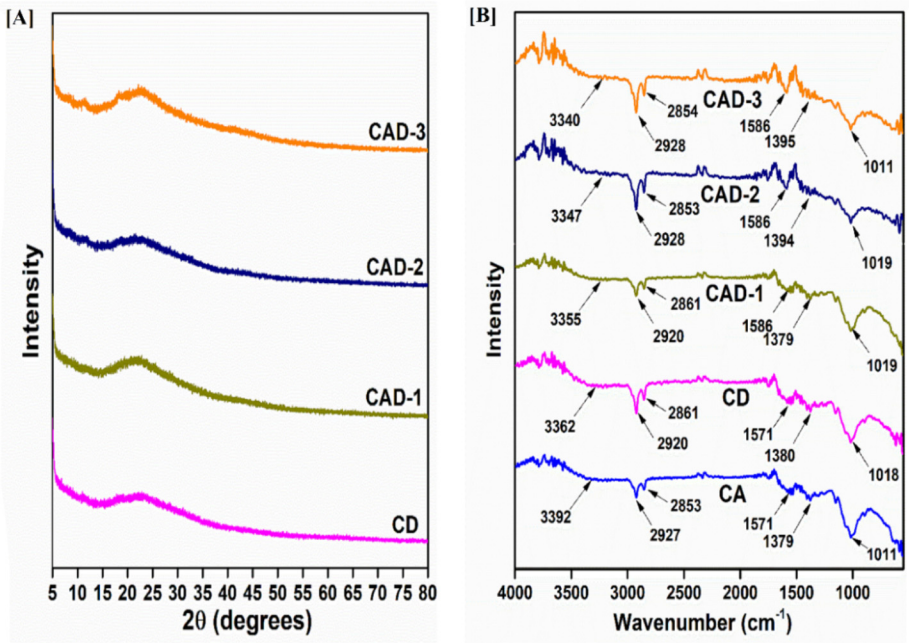

Fig. 3 [A] X-ray diffractograms and [B] FTIR spectra of the AH-loaded films.

Table 3 Thickness, crystallinity and mechanical parameters of the fabricated films

Sample code	Thickness (mm)	Crystallinity percentage (%) as calculated from XRD	Crystallinity percentage (%) as calculated from DSC	Tensile strength (MPa)	Extensibility (%)
CD	0.071 ± 0.012^{a}	33.214 ± 0.153^{d}	30.178 ± 0.546^{a}	28.279 ± 0.398^{c}	11.607 ± 0.307^{d}
CAD-1	0.072 ± 0.006^{bc}	38.669 ± 0.841^{a}	37.164 ± 0.299^{c}	26.283 ± 0.648^{b}	16.128 ± 0.591^{b}
CAD-2	0.084 ± 0.014^{a}	42.147 ± 0.624^{b}	41.879 ± 0.212^{cd}	11.848 ± 0.941^{a}	19.740 ± 0.821^{a}
CAD-3	0.096 ± 0.011^{b}	52.607 ± 0.517^{bc}	51.246 ± 0.351^{b}	13.923 ± 0.164^{d}	26.731 ± 0.568^{bc}

The different superscripts in the columns indicate varied values at $p \leq 0.05$ while Tukey's test was used.

leading to a highly dense arrangement between the constituents of the film matrix. Hence this aids in increasing the crystallinity percentage of the fabricated films.

4.2.2 Spectroscopic properties. The IR spectra of the film samples provided insight into the molecular interactions taking place between the constituents of the film matrix. The FTIR spectra of the films are given in Fig. 3[B]. The relatively broader bands observed in the range 3340 cm^{-1} to 3392 cm^{-1} indicated the hydroxyl groups present in the film samples. It was observed that the –OH stretching frequency continuously decreased from the CA to CAD-3 film, indicating constructive intermolecular hydrogen bonding between CH, ABE and AH. Thus, owing to the stronger bonding, a lower mobility of the chains of CH can be observed, which is evident from the increasing degree of crystallinity of the films as displayed in Table 2. The bands associated with 2920 cm^{-1} and 2861 cm^{-1} correspond to the stretching (asymmetric and symmetric) bands of $-CH_2$ groups.[43] The bands attributed to the C=O stretching in amide-I and –OH bending are present at 1586 cm^{-1} and 1379 cm^{-1}.[44] The bands in the range 1011 to 1019 cm^{-1} were ascribed to the C–O functional groups present in the polymer matrix. There were significant changes in the wavenumbers of the functional groups, indicating potential interactions between the components of the polymer matrix.

4.2.3 Thickness and mechanical properties. Films of a definite thickness are prerequisites for suitable applications. It was observed that the control film containing AH exhibited the lowest thickness. The thicknesses of the films are provided in Table 3. The addition of the ABE to the CH matrix exhibited an increase in the thickness. This progression could be on account of the irregularity in the polymeric backbone of CH induced by the addition of the ABE.[45] The phenolic compounds present in the ABE confer a plasticizing effect on the CH matrix, thereby increasing the thickness of these films gradually with an increase in the concentration of the extract.[46]

The mechanical properties of the films are displayed as stress–strain curves in Fig. 4[A]. The values of the parameters of mechanical properties such as tensile strength and extensibility are tabulated in Table 3. The films employed for drug delivery may be subjected to human body environments involving stress, which may lead to the disintegration of the films.

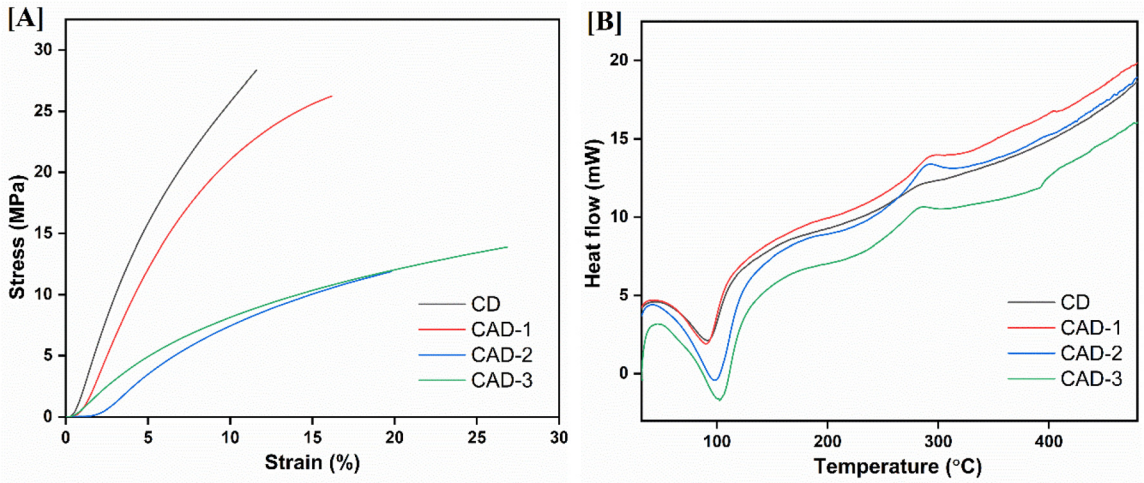

Fig. 4 [A] Stress–strain curves and [B] DSC thermograms of the AH-loaded films.

Hence, an examination of the mechanical parameters of the films is necessarily done to discern this factor.[47] The control chitosan film (CD) demonstrated the highest tensile strength of 28.279 MPa, indicative of a rigid, hydrogen-bonded network. While the ABE incorporated films showed a decline in tensile strength, the extensibility of the films increased with increasing ABE concentration. The decrease in tensile strength could be ascribed to the discontinuity in the chains of CH induced by the ABE. This apparently causes the matrix to resist any fracture.[48] Hence, the tensile strength of the films reduces on moving from the CAD-1 to CAD-3 films. While the increment in extensibility can be linked to the plasticising ability of the ABE, the polyphenols present in the ABE may have contributed to this extensibility[49] The CAD-1 film exhibited the most balanced performance, maintaining relatively higher stiffness while accommodating deformability, whereas excessive plasticization effects dominated CAD-2 and CAD-3.

4.2.4 Thermal stability. The thermal stability of the films was examined using the DSC thermograms shown in Fig. 4[B]. From the thermograms, it is clearly observable that there is a presence of a sharp glass transition temperature (T_g), implying miscibility of the blended components.[50] The T_g of the control CD film was found to be 91.08 °C, while the ABE incorporated films exhibited T_g of 89.8 °C, 97.5 °C and 101.7 °C for the CAD-1, CAD-2 and CAD-3 films respectively. This indicates that there has been stronger CH/ABE/AH bonding, leading to pronounced T_g values.[51]With regard to the melting temperatures (T_m), it has been identified that the drug AH melts at 177 °C,[52] considering previous research. However, as shown in the thermograms, the T_m of the films was observed to be in the range 281 °C to 293 °C, implying a stronger network between the blended components. Also, the presence of a single melting peak indicates that AH was molecularly dispersed in the CH/ABE matrix.[53] The crystallinity of the films was also evaluated using the DSC thermograms and the values are tabulated in Table 3. From Table 3, it was found that there were not much distinct differences between the crystallinity values obtained from the two modes of analysis, confirming the increasing crystalline nature of the films.

4.2.5 Morphology of the film surfaces. The morphological features of the tailored films can be observed in the SEM images provided in Fig. 5. These observations indicate that the CD film containing only the base matrix CH and the drug AH possesses a surface containing a large number of pores that are larger in size. While the films containing varying increasing concentrations of ABE have shown that the number of pores has been minimised, the film containing the highest concentration of the extract shows the absence of pores. The bright particles present on the surface of the films appeared to be the undissolved particles of CH; however, there was no phase separation, indicating complete miscibility of the blended components. These observations are similar to those reported by Tuhin *et al.*[54] and Yadav *et al.*[55] Overall, the micrographs provide a morphological outline, implying that the progression in ABE concentration results in the development of denser films with a reduction in porosity on advancing from CAD-1 to CAD-3. These observations are in conformity with the XRD and FTIR studies, which indicate that the blended components are bonded strongly with an increase in ABE concentration.

4.2.6 Hydrophobicity of the films. Water contact angle measurements shown in Fig. 6 indicate that the wettability of the CH/ABE/AH films is strongly dependent on ABE loading. The pristine chitosan film (CD) exhibited a contact angle of 82.2°, reflecting a moderately hydrophilic surface governed by polar amino and hydroxyl functionalities.[56] Incorporation of ABE reduced the angle to 79.7° in CAD-1, suggesting increased surface polarity, either by the migration of ABE-derived groups to the film surface or by topographical changes that favored water spreading. A further decrease was observed in CAD-2 (~71.7°), consistent with the greater availability of hydrophilic moieties and partial disruption of surface-ordered domains.[57]

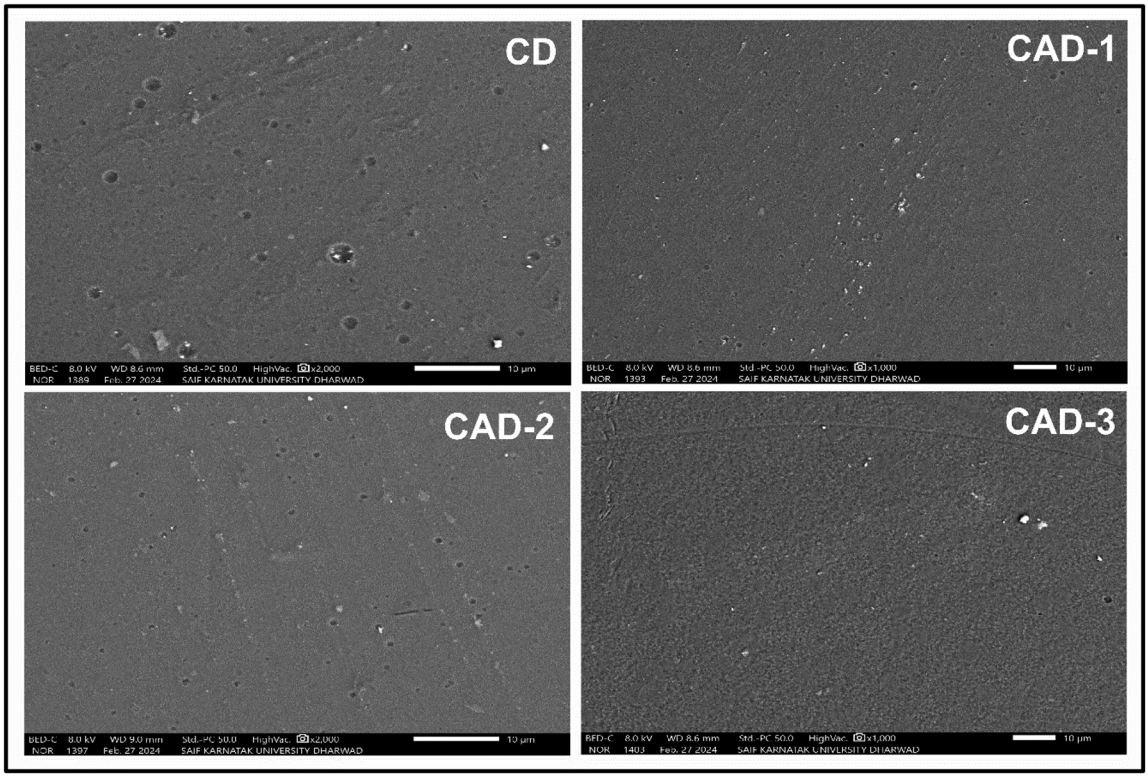

Fig. 5 Morphological images of the films.

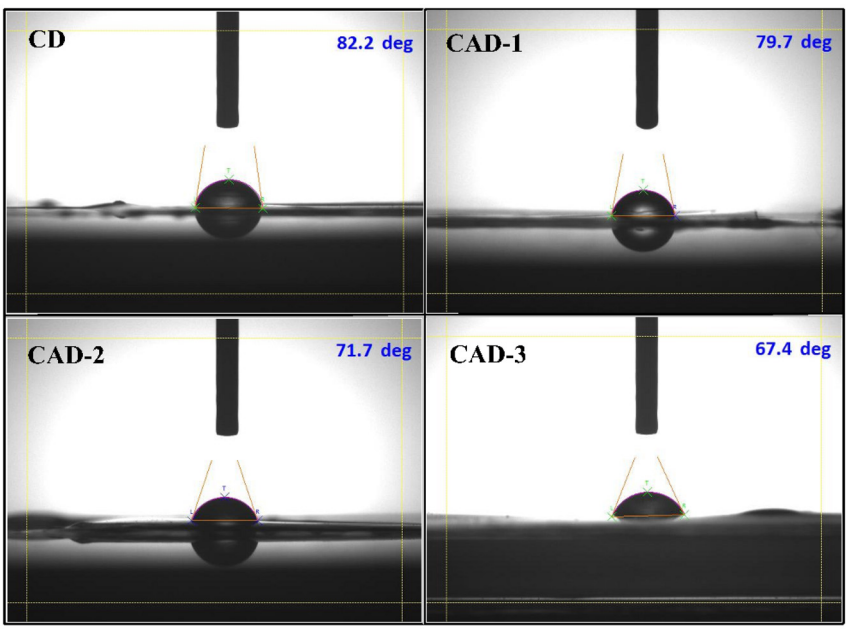

Fig. 6 Measurement of the water contact angles of the films.

At the highest ABE loading (CAD-3), the contact angles stabilized around ~67.4°, indicating that additional ABE no longer increased hydrophilicity, likely due to the surface saturation or formation of heterogeneous domains.[58] The presence of AH produced only a secondary effect, enhancing hydrophilicity at lower ABE concentrations but becoming negligible once ABE dominated the surface composition.[59,60] These observations align with the reported behavior of chitosan composites con-

taining plant-derived additives, where initial additive incorporation enhances surface polarity, but excessive loading induces phase segregation or competing surface chemistries that limit further reductions in contact angle.

4.2.7 Swelling behaviour of the films. The study of the swelling behavior of films is vital for their application in drug delivery. The interactions between the polymer, drug and intestinal fluids decide the rate of drug release from the host matrix. The swelling behavior of the films was analyzed at room temperature in a PBS solution at pH 7.4 and the results are shown in Fig. 7[A] and [B]. The swelling behavior was noted every 30 min during the initial 4 h, then the samples were evaluated after an hour for up to 48 h. The swelling of the control CD film could be attributed to the polar groups present in the backbone of CH.[61] The rate of swelling of the drug-loaded films decreased with the addition of ABE. The higher concentrations of ABE contain higher concentrations of negatively charged compounds that may possibly interact with the functional groups of CH that are positively charged, resulting in reduced swelling of films due to the hindrance in the movement of chains.[62] Chin *et al.* also reported a similar swelling behavior of films.[63] The higher concentration of ABE may have caused the formation of stronger bonds between CH and ABE, leaving lesser space for swelling. These results are supported by the XRD analysis which shows that the compactness and high crystallinity associated with the increasing concentration of the ABE leaves fewer voids for the accumulation of –OH functional groups. This is also supported by the SEM results. The highest rate of swelling was observed for the CAD-1 film which contained the lowest concentration of ABE. The swelling capacity of the films followed the order: CAD-1 > CAD-2 > CAD-3 > CD.

4.2.8 *In vitro* release studies. The *in vitro* release behavior of a drug over a definite time period is an important criterion for designing films for drug delivery applications. In the current study, emphasis was laid on studying the release of the drug AH from the CH/ABE matrix over a period of 24 h. The release behavior of AH from the films is shown in Fig. 8. The release analysis revealed that the amount of AH leaching out of the film matrix consistently followed the trend of the swelling behavior of the film. With an increase in the concentration of ABE, the release behavior of the films followed sustained behavior. The initial sudden eruption of the drug from the film was noticed, which could be linked to the expeditious swelling of the film samples, allowing smooth diffusion of AH due to loosening of the bonds on swelling. Another reason could be the adsorption of the drug onto the film surface. Apparently, the loosely bound molecules of AH at the surface of the films may have drifted away, leading to the initial rapid burst.[64] However, with increasing time, the CAD-3 film showed modest and controlled release of the drug from the matrix. This could

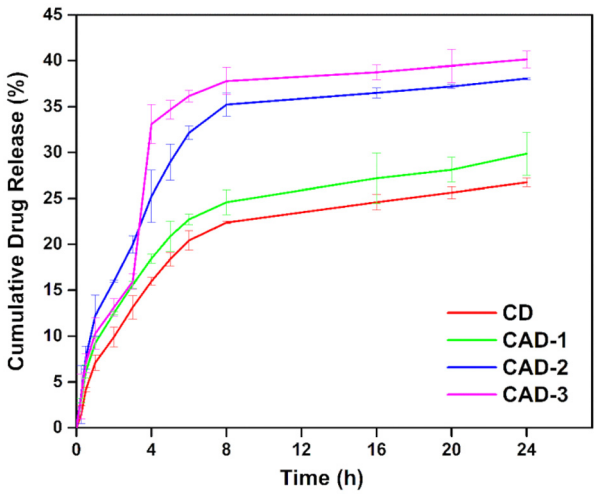

Fig. 8 Drug release profiles of the CD, CAD-1, CAD-2 and CAD-3 films for a period of 24 hours.

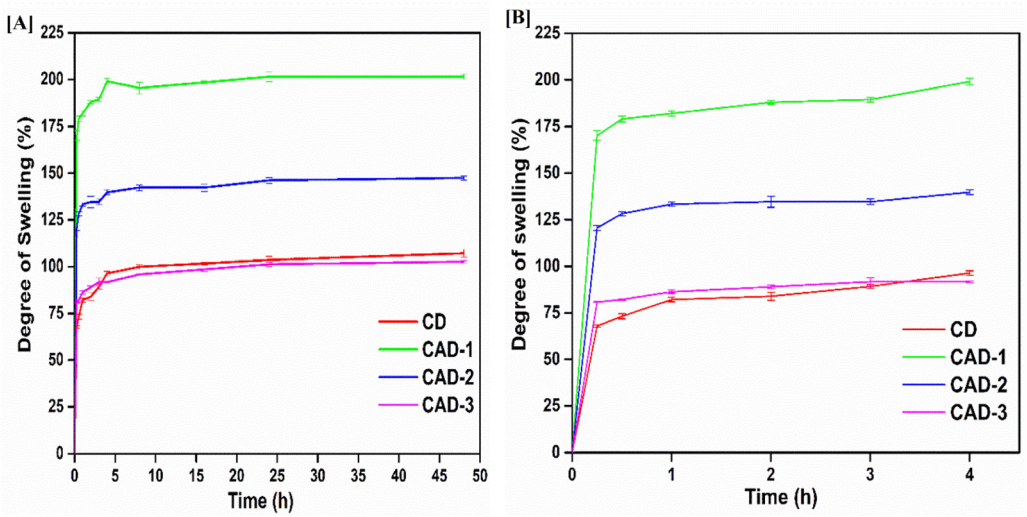

Fig. 7 [A] Overall swelling behaviour of the films from initial time to 48 hours and [B] initial swelling behaviour of the films up to 4 hours.

be due to the good synergy between the positively charged groups of CH and the negatively charged groups of ABE, inducing a steady release of the drug, AH.[62,64] On the other hand, the CAD-2 and CAD-3 films again showed a second sudden burst of AH at the 4th hour. This could be linked to their compact morphology and minimization of pores in the film matrix which are evident in the SEM micrographs. At higher concentrations of ABE, there has been an increase in the rate of swelling as observed in the swelling studies. Due to this, the already existing compact morphology may have been disturbed on account of the internal stress and cracking of the matrix, thereby causing rapid leaching of the drug,[65] thus leading to ineffective controlled release. However, from Fig. 8, it is evident that CAD-1 released almost 25% of the drug AH loaded onto the film within a time interval of 24 hours. This signifies that there is a controlled release of the drug AH from the film matrix, which allows a tunable release capacity and allows these films to be harnessed in controlled drug delivery systems. Table 7 gives comprehensive details comparing the present work with the previously reported works. In addition to this, the phenomenon of relaxation of polymer chains which is related to the swelling behaviour of the films is also observed in the release rate analysis. The CH/ABE/AH network is disrupted on the uptake of PBS, leading to spikes in release rates. The early burst is driven by the diffusion of adsorbed AH molecules onto the surface of the CH/ABE matrix, followed by the polymer relaxation observed in CD and CAD-1, owing to the presence of free volume between the polymer chains which is in accordance with SEM micrographs depicting higher numbers of pores, while the second burst, mainly occurring in the CAD-2 and CAD-3 films, results in disruption in the relaxation of polymer chains due to the minimum free space because of the stronger CH/ABE/AH bonding. This can be attributed to the pore minimisation in the SEM micrographs. This clearly explains the effective controlled release pattern of the CAD-1 film in conformity with the FTIR spectra, XRD diffractograms and SEM micrographs. This also highlights the superiority of this film over the CAD-2 and CAD-3 films.

4.2.9 Loading efficiency of the films. The ability of the film samples to accommodate a certain quantity of the drug AH was readily evaluated. The higher the drug loading ability, the lower the amount of polymer required to form the film.[66] Table 4 shows the drug loading capacities of the films. It was found that the CD film contained the highest capacity to hold the drug, while the loading capacity slowly retarded with increasing concentrations of ABE, although not appreciably. The larger size of the molecules of the compounds of ABE could have possibly led to the reduced capacity to withhold the drug, which is evident from the increasing thickness of the films. This is also supported by the micrographs of SEM, which indicate that the CD and CAD-1 films show a large number of pores in their matrix, accounting for free space for entrapment of AH. Hence, the loading capacity is the highest for these films. The EE values of the films are also presented in Table 4. The EE values of the films show a slight deviation from the drug loading capacity, whereas the CAD-1 film shows the maximum EE. This possibly indicates that the CAD-1 film containing the minimum concentration of ABE has good efficiency in encapsulating the drug, thereby permitting only a controlled amount of drug AH to be released at certain intervals, which was discerned from the release studies of AH from the film samples. The strong CH/ABE/AH network as indicated by FTIR and the affinity between the oppositely charged groups of CH and ABE could have given rise to a stronger network, thereby effectively encapsulating the drug AH.[67]

4.2.10 Drug release kinetics. One of the most important criteria required for an ideal drug delivery system is to harmonically deliver the drug at the required rate suiting the needs of the individual undergoing treatment. This leads to therapeutic efficacy and a reduction in the number of dosages required.[68] In order to determine this efficacy, the mechanism of the release of the drug AH from the polymer matrix CS/ABE was analyzed by fitting the cumulative drug release data to various mathematical models. Concerning polymer matrix systems, the diffusion of the drug and the relaxation of the polymer chains control the release rate of the drug. Table 5 provides detailed values of the release profiles using several kinetic models.

Zero-order kinetics mainly implies the dissolution of the drug at a slower pace, avoiding the consequences of disaggregation. Drug-delivery systems based on this model are known for their prolonged pharmacological activity.[69] A straight line was obtained for the zero-order release equation, with correlation coefficients (R^2) ranging from 0.72 to 0.82. The CAD-1 sample showed a higher R^2 value in this regard, apparently indicating its use for sustained release. The minimal variations obtained in the values of the zero-order rate constant K could be ascribed to the seeping out of the drug AH with a reduced velocity induced by the CS/ABE matrix.[70]

The first-order kinetics model depicts the absorption or elimination of a water-soluble drug from the matrix based on the porosity and density of the drug-delivery system.[69] From Table 5, it is evident that the values of R^2 vary widely, indicating that the concentration of AH is independent of the matrix involved. Since AH is highly water soluble and the CS/ABE blend matrix is porous, it causes the rapid dissolution of AH as soon as the solvent medium penetrates the blend matrix.[71] On the lines of the Higuchi model, the R^2 values of the CAD-1 film confirm the fact that the release of drug AH is driven by

Table 4 Drug loading capacity and encapsulation efficiency (EE) values of the AH-loaded films

Sample code	Drug loading capacity (%)	Encapsulation efficiency (EE) (%)
CD	82.165 ± 0.084^{a}	15.318 ± 0.042^{a}
CAD-1	78.662 ± 0.031^{c}	19.012 ± 0.027^{c}
CAD-2	76.751 ± 0.068^{b}	11.082 ± 0.008^{d}
CAD-3	75.159 ± 0.017^{d}	9.777 ± 0.039^{ab}

The different superscripts present in the columns indicate that the values are significantly ($p \leq 0.05$, analysis was done in triplicate) different from each other.

Table 5 The kinetic parameters were derived by fitting the mathematical models of the AH release profiles from the CS/ABE matrices

	Zero-order model		First-order model		Higuchi model		Korsmeyer–Peppas model		
Sample code	R^2	K	R^2	K	R^2	K	R^2	K	n
CD	0.817	5.225	0.888	0.138	0.942	2.509	0.918	0.439	0.627
CAD-1	0.893	5.453	0.515	0.115	0.946	2.610	0.946	1.044	0.504
CAD-2	0.776	7.089	0.609	0.117	0.916	3.484	0.931	1.225	0.527
CAD-3	0.722	7.874	0.778	0.131	0.867	3.937	0.906	0.909	0.584

Table 6 Diameters (in mm) of the zones of inhibition of the *E. coli* and *S. aureus* bacteria

Sample code	*E. coli*	*S. aureus*
CD	5 ± 0.01^{d}	2 ± 0.06^{ab}
CAD-1	7 ± 0.04^{b}	3 ± 0.08^{a}
CAD-2	9 ± 0.02^{c}	4 ± 0.01^{c}
CAD-3	12 ± 0.07^{a}	—

Different superscripts within the columns specify that the values are significantly different ($p \leq 0.05$, $n = 3$).

the process of diffusion from the CH/ABE matrix. The minimal concentration of ABE in the CAD-1 film allows for the uptake of aqueous media (in this case, PBS), allowing the drug AH to leach out efficiently from the film matrix.

The Korsmeyer–Peppas model is applicable when more than one release mechanism occurs in the drug-delivery system. The release exponent 'n' has shown values greater than 0.5, indicating anomalous non-Fickian diffusion.[72] This is indicative of the fact that matrix swelling and diffusion of the drug occur simultaneously.[73] The constant values of R^2 signify the controlled release of AH from the polymer matrix, with CAD-1 showing steady dissolution. From the analysis of these mathematical models, it can be inferred that a lower concentration of ABE allows for smooth dissolution of the drug AH from the CS/ABE matrix at a sustained rate. Also, the minimal increment in the value of n from CAD-1 to CAD-3 could be due to the good anchorage of the bonds between various components of the matrix, as sufficed by FTIR and XRD results, which imply stronger intermolecular CH/ABE/AH interactions with increasing ABE concentration. The observations are consistent with previous reports on CH-based films whose release kinetics followed the exhibited Korsmeyer–Peppas model depicting anomalous non-Fickian diffusion.[74–76]

4.2.11 Cytotoxicity behaviour of the films. Cytotoxicity is a crucial parameter for determining the efficacy of biomaterials as safe materials for human use. It also intends to indicate the biocompatibility of the biomaterials fabricated with animal cells. Fig. 9 shows the cell viability percentages of the drug-loaded films which were readily evaluated using mouse skin fibroblast L929 cell lines. It is evident that all the films exhibited good cytotoxicity behavior, making them favorable for use as biomaterials (cell viability > 75%).[77]

The percentage of cell viability was investigated for the films without ABE, *i.e.* the control CD film, and for those including ABE (CAD-1, CAD-2, CAD-3). The control CD film showed the highest percentage of cell viability. Furthermore, the percentage of cell viability appeared to increase with the increasing concentration of ABE to a value of 91% for the CAD-2 film and then there was a decrease in the cell viability for the CAD-3 film. The phytochemicals may have been responsible for this progression, which may have aided in keeping the cells active, rather than hindering their activity. The slight decrease in cell viability percentage at the higher concentration of ABE could be ascribed to the presence of certain con-

Table 7 Comparison of the drugs used, film compositions, recommended treatments and key findings of films used for controlled release of drugs

Drug used	Film composition	Key findings	Limitations	Ref.
Norfloxacin (antibacterial)	CH + halloysite nanotubes	• Controlled release achieved • Release rate: >45% in 6 h	• Early burst release rate: (>30% in 1 h) • Use of halloysite nanotubes as drug carriers and then introduction in films	23
Ciprofloxacin (antibacterial)	CH + ciprofloxacin + glutaraldehyde	• Controlled release achieved • Release rate: >60% in 24 h	• Early burst release rate: (>60% in 4 h) • Use of a synthetic crosslinking agent	7
Doxorubicin hydrochloride (anticancer)	CH	• Controlled release achieved • Release rate: >60% in 6 h	• Early burst release rate: (>20% in 1 h) • Use of a synthetic crosslinking agent	81
5-Fluorouracil (anticancer)	CH + banana peel extract	• Controlled release achieved • Release rate: >55% in 24 h • Use of natural extract in developing films	• Early burst release rate: (>25% in 5 h)	6
Acebutolol hydrochloride (cardioselective β-blocker)	CH + *Averrhoa bilimbi* leaf extract	• Controlled release achieved • Release rate: >25% in 24 h • Use of natural extract in developing films	• Partial drug release • Secondary burst at high concentrations of ABE	Present work

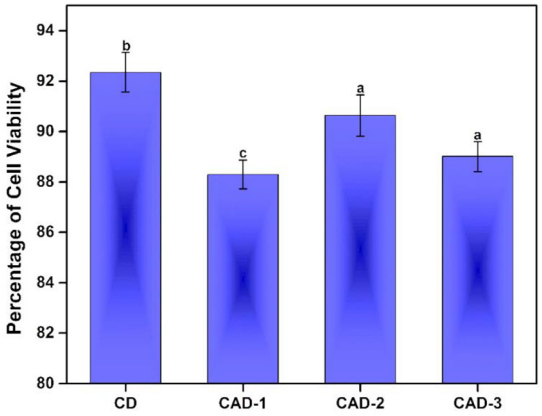

Fig. 9 Cell viability percentages of the AH loaded CH/ABE films.

stituents in the ABE, which may have hindered cell activities.[78] These results confirm the non-toxic nature of the CH/ABE matrix, while also indicating that the incorporation of ABE did not induce any detrimental effects, supporting their applicability as drug-delivery films.

4.2.12 Bacterial resistance of the films. The efficiencies of the drug-loaded films in inhibiting bacterial growth are presented in Fig. 10 and are tabulated in Table 6. The inhibition zones were investigated against Gram-positive *S. aureus* and Gram-negative *E. coli*. It was found that the control CD film showed good bacterial resistance due to the inherent antibacterial nature of the polysaccharide CH. The zones of inhibition for *E. coli* bacteria were found to be prominent with increases in the ABE content. The polyphenols present in the ABE may restrict the growth of bacteria and disrupt cell functioning. This also provides insight into the diffusivity of the active contents of the ABE from the CH matrix into the diffusion medium. The higher the concentration of ABE, the greater the diffusivity, which aids the effective release of the drug. The relatively lower inhibition towards *S. aureus* could be due to its Gram-positive nature which possesses numerous layers of peptidoglycan, making it harder for the contents of the film matrix to seep into this bacteria.[79] The CAD-3 film showed the absence of an inhibition zone for *S. aureus* bacteria which could be due to the excess concentration of ABE reducing the speed of migration of the contents from the film to the diffusion media owing to its large volume.[80] However, there was no growth of bacteria on the film, proving it to be bacteriostatic in nature.

4. Conclusions

Acebutolol hydrochloride (AH)-loaded chitosan (CH)/*Averrhoa bilimbi* leaf extract (ABE) films demonstrated exceptional potential as controlled delivery systems for the β-blocker AH. The films were fabricated *via* a simple and effective solvent evaporation method using biodegradable and biocompatible materials such as CH and ABE. Notably, the films exhibited

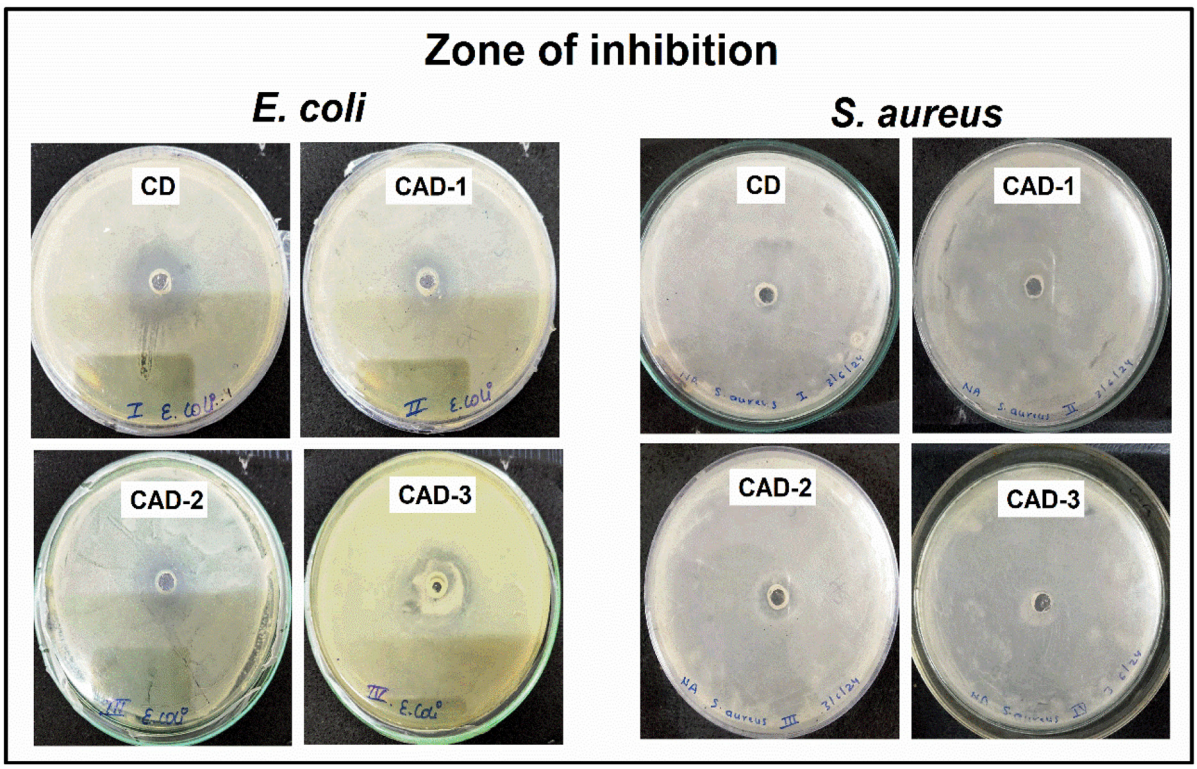

Fig. 10 Images depicting bacterial zones of inhibition of the CD, CAD-1, CAD-2 and CAD-3 films.

increased thickness and enhanced crystallinity, indicating a high level of compatibility between the matrix constituents. Spectroscopic analysis, coupled with microscopic imaging, further corroborated these findings. The FTIR spectra revealed stronger hydrogen bonding, while the SEM images displayed a homogeneous surface morphology, underscoring the uniform integration of the components. The films exhibited increasing flexible nature along with pronounced thermal stability. Evaluation of the films' swelling indices, sustained drug release rates, and drug loading efficiencies suggests that these films are highly effective in modulating the release profile of the β-blocker AH, thereby reducing the frequency of drug administration and mitigating potential adverse health effects. The inclination of the release rates of the developed films towards the Higuchi and Korsmeyer–Peppas models suggests that AH is released *via* non-Fickian diffusion, highlighting that the release phenomenon is a simultaneous occurrence of both the swelling of the CH/ABE matrix and diffusion of AH from the matrix. Thus, the biocompatibility and bacterial resistance of the films further confirm their safety for human use, positioning them as promising options for controlled drug delivery applications.

Author contributions

Jennifer P. Pinto: conceptualization, data interpretation, and writing – original manuscript. Manjunath B. Megalamani: design of the study and methodology. Ajitkumar Appayya Hunashyal: investigation and formal analysis. Oshin Jacintha D'souza: visualisation and data curation. Sharanappa T. Nandibewoor: supervision and validation. Saraswati P. Masti: revising manuscript. Ravindra B. Chougale: supervision, correspondence, review, and formal correction.

Conflicts of interest

All authors declare no conflicts of interest.

Data availability

The data supporting the findings of this study will be made available from the corresponding author upon reasonable request.

Acknowledgements

One of the authors, Jennifer P. Pinto, acknowledges financial support from the University Grants Commission, Government of India, through the Savitribai Jyotirao Phule Single Girl Child Fellowship (SJSGC) – 2023 (Ref. No. UGCES-22-OB-KAR-F-SJSGC-2368). The authors gratefully acknowledge the Sophisticated Analytical Instrument Facility (SAIF), and University Scientific Instrumentation Centre (USIC), Karnatak University, Dharwad, for providing necessary instrumentation amenities.

References

1 K. K. Jain, *An Overview of Drug Delivery Systems*, vol. 2059. 2020. DOI: 10.1007/978-1-4939-9798-5_1.
2 V. S. Bheemidi, M. Tiruckovela and P. Varanasi, An imperative note on novel drug delivery systems, *J. Nanomed. Nanotechnol.*, 2011, **2**, 100125.
3 S. Adepu and S. Ramakrishna, Controlled drug delivery systems: Current status and future directions, *Molecules*, 2021, **26**(19), DOI: 10.3390/molecules26195905.
4 D. Liu, F. Yang, F. Xiong and N. Gu, The smart drug delivery system and its clinical potential, *Theranostics*, 2016, **6**(9), 1306–1323, DOI: 10.7150/thno.14858.
5 T. Gazori, M. R. Khoshayand, E. Azizi, P. Yazdizade, A. Nomani and I. Haririan, Evaluation of Alginate/Chitosan nanoparticles as antisense delivery vector: Formulation, optimization and in vitro characterization, *Carbohydr. Polym.*, 2009, **77**(3), 599–606, DOI: 10.1016/j.carbpol.2009.02.019.
6 D. Radha, J. S. Lal and K. S. Devaky, Release studies of the anticancer drug 5-fluorouracil from chitosan-banana peel extract films, *Int. J. Biol. Macromol.*, 2024, **256**, 128460.
7 S. Affes, I. Aranaz, N. Acosta, Á. Heras, M. Nasri and H. Maalej, Chitosan derivatives-based films as pH-sensitive drug delivery systems with enhanced antioxidant and antibacterial properties, *Int. J. Biol. Macromol.*, 2021, **182**, 730–742, DOI: 10.1016/j.ijbiomac.2021.04.014.
8 N. Samiraninezhad, K. Asadi, H. Rezazadeh and A. Gholami, Using chitosan, hyaluronic acid, alginate, and gelatin-based smart biological hydrogels for drug delivery in oral mucosal lesions: A review, *Int. J. Biol. Macromol.*, 2023, 126573.
9 E. Pezik, T. Gulsun, S. Sahin and İ. Vural, Development and characterization of pullulan-based orally disintegrating films containing amlodipine besylate, *Eur. J. Pharm. Sci.*, 2021, **156**, DOI: 10.1016/j.ejps.2020.105597.
10 T. Maver, *et al.*, Cellulose based thin films as a platform for drug release studies to mimick wound dressing materials, *Cellulose*, 2015, **22**(1), 749–761, DOI: 10.1007/s10570-014-0515-9.
11 J. S. Boateng, H. V. Pawar and J. Tetteh, Polyox and carrageenan based composite film dressing containing antimicrobial and anti-inflammatory drugs for effective wound healing, *Int. J. Pharm.*, 2013, **441**(1–2), 181–191, DOI: 10.1016/j.ijpharm.2012.11.045.
12 F. Tao, *et al.*, Chitosan-based drug delivery systems: From synthesis strategy to osteomyelitis treatment – A review, *Carbohydr. Polym.*, 2021, **251**, 117063, DOI: 10.1016/j.carbpol.2020.117063.
13 R. Jayakumar, M. Prabaharan, P. T. Sudheesh Kumar, S. V. Nair and H. Tamura, Biomaterials based on chitin and chitosan in wound dressing applications, *Biotechnol. Adv.*, 2011, **29**(3), 322–337, DOI: 10.1016/j.biotechadv.2011.01.005.
14 J. Potaś, E. Szymańska and K. Winnicka, Challenges in developing of chitosan – Based polyelectrolyte complexes

as a platform for mucosal and skin drug delivery, *Eur. Polym. J.*, 2020, **140**, 110020, DOI: 10.1016/j.eurpolymj.2020.110020.

15 B. Kaczmarek, A. Sionkowska, F. J. Monteiro, A. Carvalho, K. Łukowicz and A. M. Osyczka, Characterization of gelatin and chitosan scaffolds cross-linked by addition of dialdehyde starch, *Biomed. Mater.*, 2018, **13**(1), DOI: 10.1088/1748-605X/aa8910.

16 J. You, *et al.*, Quaternized Chitosan/Poly(acrylic acid) Polyelectrolyte Complex Hydrogels with Tough, Self-Recovery, and Tunable Mechanical Properties, *Macromolecules*, 2016, **49**(3), 1049–1059, DOI: 10.1021/acs.macromol.5b02231.

17 H. Y. Setyawan, S. Sukardi and B. F. Nareswari, The phytochemical potential of Averrhoa bilimbi - A review, *IOP Conf. Ser.: Earth Environ. Sci.*, 2021, **733**(1), DOI: 10.1088/1755-1315/733/1/012091.

18 A. C. Iwansyah, *et al.*, Evaluation on the physicochemical properties and mineral contents of Averrhoa bilimbi L. leaves dried extract and its antioxidant and antibacterial capacities, *Food Sci. Technol.*, 2021, **41**, 987–992.

19 A. Radha, A. Singh, L. Sharma and K. K. Thakur, Molecular interactions of acebutolol hydrochloride to human serum albumin: A combined calorimetric, spectroscopic and molecular modelling approach, *Mater. Today: Proc.*, 2021, **44**, 1700–1706, DOI: 10.1016/j.matpr.2020.11.872.

20 Y. N. Patil, M. B. Megalamani and S. T. Nandibewoor, PVA Capped Mn-Doped ZnS Encapsulated Nontoxic MoS 2 Nano-Sheet Probe for the Sensitive Estimation of Cardiovascular β-Blocking Agent Acebutolol in Biomedical and Environmental Samples, *J. Electrochem. Soc.*, 2023, **170**(3), 037505, DOI: 10.1149/1945-7111/acbe6d.

21 K. Boussery, F. M. Belpaire and J. Van de Voorde, *Physiological Aspects Determining the Pharmacokinetic Properties of Drugs*, Elsevier Ltd, 2008. DOI: 10.1016/B978-0-12-417205-0.00023-7.

22 A. Z. Ranjitha and N. G. N. Swamy, Formulation and in vitro evaluation of acebutolol hydrochloride microballoons for sustained drug delivery, *Indian J. Novel Drug Deliv.*, 2014, **6**(2), 124–131. Available: https://www.embase.com/search/results?subaction=viewrecord&from=export&id=L604474738.

23 M. Barman, S. Mahmood, R. Augustine, A. Hasan, S. Thomas and K. Ghosal, Natural halloysite nanotubes /chitosan based bio-nanocomposite for delivering norfloxacin, an anti-microbial agent in sustained release manner, *Int. J. Biol. Macromol.*, 2020, **162**, 1849–1861, DOI: 10.1016/j.ijbiomac.2020.08.060.

24 L. Valero, M. Gainche, C. Esparcieux, F. Delor-Jestin and H. Askanian, Vegetal Polyphenol Extracts as Antioxidants for the Stabilization of PLA: Toward Fully Biobased Polymer Formulation, *ACS Omega*, 2023, **9**(7), DOI: 10.1021/acsomega.3c07236.

25 J. P. Pinto, *et al.*, Development of Chitosan-Copovidone nanocomposite films with antioxidant and antibacterial properties for food packaging applications, *Food Hum.*, 2023, **1**, 378–390, DOI: 10.1016/j.foohum.2023.06.003.

26 S. S. Narasagoudr, Y. Shanbhag, R. B. Chougale, B. M. Baraker, S. P. Masti and B. Lobo, Thermal degradation kinetics of ethyl vanillin crosslinked chitosan/poly(vinyl alcohol) blend films for food packaging applications, *Chem. Data Collect.*, 2021, **34**, DOI: 10.1016/j.cdc.2021.100739.

27 J. Chalitangkoon, M. Wongkittisin and P. Monvisade, Silver loaded hydroxyethylacryl chitosan/sodium alginate hydrogel films for controlled drug release wound dressings, *Int. J. Biol. Macromol.*, 2020, **159**, 194–203, DOI: 10.1016/j.ijbiomac.2020.05.061.

28 A. B. Reddy, B. Manjula, T. Jayaramudu, E. R. Sadiku, P. Anand Babu and S. Periyar Selvam, 5-Fluorouracil Loaded Chitosan–PVA/Na + MMT Nanocomposite Films for Drug Release and Antimicrobial Activity, *Nano-Micro Lett.*, 2016, **8**(3), 260–269, DOI: 10.1007/s40820-016-0086-4.

29 A. M. Craciun, L. Mititelu Tartau, M. Pinteala and L. Marin, Nitrosalicyl-imine-chitosan hydrogels based drug delivery systems for long term sustained release in local therapy, *J. Colloid Interface Sci.*, 2019, **536**, 196–207, DOI: 10.1016/j.jcis.2018.10.048.

30 O. Jacintha, T. Gasti, V. Hiremani, J. Pinto, S. Contractor, A. Shettar, D. Olivia, S. Arakera, S. Masti, R. Chougale, *et al.*, International Journal of Biological Macromolecules Basella alba stem extract integrated poly (vinyl alcohol)/chitosan composite films: A promising bio-material for wound healing, *Int. J. Biol. Macromol.*, 2023, **225**, 673–686, DOI: 10.1016/j.ijbiomac.2022.11.130.

31 L. Monjazeb Marvdashti, A. Koocheki and M. Yavarmanesh, Characterization, Release Profile and Antimicrobial Properties of Bioactive Polyvinyl Alcohol-Alyssum homolocarpum Seed Gum- Nisin Composite Film, *Food Biophys.*, 2019, **14**(2), 120–131, DOI: 10.1007/s11483-018-09562-y.

32 M. R. R. Rahardhian, B. T. Murti, D. Wigati, R. Suharsanti and C. N. Putri, Solvent concentration effect on total flavonoid and total phenolic contents of Averrhoa bilimbi leaf extract, *Pharmaciana*, 2019, **9**(1), 137–144, DOI: 10.12928/pharmaciana.v%vi%i.10809.

33 M. T. Islam, *et al.*, Phytol: A review of biomedical activities, *Food Chem. Toxicol.*, 2018, **121**, 82–94, DOI: 10.1016/j.fct.2018.08.032.

34 M. L. Gonzalez-Rivera, J. C. Barragan-Galvez, D. Gasca-Martínez, S. Hidalgo-Figueroa, M. Isiordia-Espinoza and A. J. Alonso-Castro, In Vivo Neuropharmacological Effects of Neophytadiene, *Molecules*, 2023, **28**(8), DOI: 10.3390/molecules28083457.

35 S.-K. Kim and F. Karadeniz, Chapter 14 - Biological Importance and Applications of Squalene and Squalane, in *Advances in Food and Nutrition Research*, ed. S.-K. Kim, Academic Press, 2012, vol. 65, pp. 223–233. DOI: 10.1016/B978-0-12-416003-3.00014-7.

36 A. O. Nogueira, Y. I. S. Oliveira, B. L. Adjafre, M. E. A. de Moraes and G. F. Aragão, Pharmacological effects of the isomeric mixture of alpha and beta amyrin from *Protium heptaphyllum* : a literature review, *Fundam. Clin. Pharmacol.*, 2019, **33**(1), 4–12, DOI: 10.1111/fcp.12402.

37 S. D. Ambavade, A. V. Misar and P. D. Ambavade, *Pharmacological, nutritional, and analytical aspects of β-sitosterol: A review*, 2014, Kluwer Academic Publishers. DOI: 10.1007/s13596-014-0151-9.
38 R. Ashraf and H. N. Bhatti, Chapter 10 – Stigmasterol, in *A Centum of Valuable Plant Bioactives*, ed. M. Mushtaq and F. Anwar, Academic Press, 2021, pp. 213–232. DOI: 10.1016/B978-0-12-822923-1.00019-4.
39 B. Al-Hindi, N. A. Yusoff, I. J. Atangwho, M. Ahmad, M. Z. Asmawi and M. F. Yam, A Soxhlet extract of Gongronema latifolium retains moderate blood glucose lowering effect and produces structural recovery in the pancreas of STZ-induced diabetic rats, *Med. Sci.*, 2016, **4**(2), 9.
40 B. Yerriswamy, C. L. Reddy, C. V. Prasad, M. C. S. Subha and K. C. Rao, Synthesis and characterization of sodium alginate-g-2-hydroxyethyl methacrylate interpenetrating beads for controlled release of acebutolol hydrochloride, *Des. Monomers Polym.*, 2011, **14**(1), 25–37, DOI: 10.1163/138577210X541178.
41 P. Ramakrishna, B. Mallikarjuna, A. C. Babu, P. Sudhakar, K. C. Rao and M. C. S. Subha, Interpenetrating polymer network of crosslinked blend microspheres for controlled release of acebutolol HCl, *J. Appl. Pharm. Sci.*, 2011, **1**(6), 212–219.
42 S. B. Aziz, Modifying Poly(Vinyl Alcohol) (PVA) from Insulator to Small-Bandgap Polymer: A Novel Approach for Organic Solar Cells and Optoelectronic Devices, *J. Electron. Mater.*, 2016, **45**(1), 736–745, DOI: 10.1007/s11664-015-4191-9.
43 S. S. Narasagoudr, V. G. Hegde, V. N. Vanjeri, R. B. Chougale and S. P. Masti, Ethyl vanillin incorporated chitosan/poly(vinyl alcohol) active films for food packaging applications, *Carbohydr. Polym.*, 2020, **236**, 116049, DOI: 10.1016/j.carbpol.2020.116049.
44 D. I. Chan-Matú, V. M. Toledo-López, M. d. L. V. y. Vargas, S. Rincón-Arriaga, A. Rodríguez-Félix and T. J. Madera-Santana, Preparation and characterization of chitosan-based bioactive films incorporating Moringa oleifera leaves extract, *J. Food Meas. Charact.*, 2021, **15**(5), 4813–4824, DOI: 10.1007/s11694-021-01055-w.
45 K. Rambabu, G. Bharath, F. Banat, P. L. Show and H. H. Cocoletzi, Mango leaf extract incorporated chitosan antioxidant film for active food packaging, *Int. J. Biol. Macromol.*, 2019, **126**, 1234–1243, DOI: 10.1016/j.ijbiomac.2018.12.196.
46 S. A. Mir, B. N. Dar, A. A. Wani and M. A. Shah, Effect of plant extracts on the techno-functional properties of biodegradable packaging films, *Trends Food Sci. Technol.*, 2018, **80**, 141–154, DOI: 10.1016/j.tifs.2018.08.004.
47 P. Ma, *et al.*, *Recent advances in mechanical force-responsive drug delivery systems*, 2022, Royal Society of Chemistry. DOI: 10.1039/d2na00420h.
48 R. B. Bodini, P. J. A. Sobral, C. S. Favaro-Trindade and R. A. Carvalho, Properties of gelatin-based films with added ethanol-propolis extract, *LWT-Food Sci. Technol.*, 2013, **51**(1), 104–110, DOI: 10.1016/j.lwt.2012.10.013.
49 V. Kola and I. S. Carvalho, *Plant extracts as additives in biodegradable films and coatings in active food packaging*, Elsevier Ltd, 2023. DOI: 10.1016/j.fbio.2023.102860.
50 J. P. Pinto, O. D'souza, V. Hiremani, N. Dalbanjan, S. Kumar, S. Narasgoudr, S. Masti, R. Chougale, *et al.*, Functional properties of taro starch reinforced polysaccharide based films for active packaging, *Food Biosci.*, 2023, **56**, 103340, DOI: 10.1016/j.fbio.2023.103340.
51 Thermal Transitions in Polymers, 1997.
52 P. Ramakrishna, B. Mallikarjuna, A. C. Babu, P. Sudhakar, M. C. S. Subha and K. C. Rao, Interpenetrating polymer network of crosslinked blend microspheres for controlled release of Acebutolol HCl, *J. Appl. Pharm. Sci.*, 2011, **1**(6), 212–219.
53 C. Venkata Prasad, B. Yerri Swamy, B. Mallikarjuna, K. Sreekanth, M. Subha, K. Chowdoji Rao, J. Yu, *et al.*, Preparation and characterization of interpenetrating polymer network beads for controlled release of acebutolol hydrochloride, *Adv. Polym. Technol.*, 2012, **31**(2), 87–99, DOI: 10.1002/adv.20238.
54 M. O. Tuhin, *et al.*, Modification of mechanical and thermal property of chitosan-starch blend films, *Radiat. Phys. Chem.*, 2012, **81**(10), 1659–1668, DOI: 10.1016/j.radphyschem.2012.04.015.
55 S. Yadav, G. K. Mehrotra, P. Bhartiya, A. Singh and P. K. Dutta, Preparation, physicochemical and biological evaluation of quercetin based chitosan-gelatin film for food packaging, *Carbohydr. Polym.*, 2020, **227**, 115348, DOI: 10.1016/j.carbpol.2019.115348.
56 X.-Y. Wang, J. Wang, C. Zhao, L. Ma, D. Rousseau and C.-H. Tang, Facile fabrication of chitosan colloidal films with pH-tunable surface hydrophobicity and mechanical properties, *Food Hydrocolloids*, 2023, **137**, 108429, DOI: 10.1016/j.foodhyd.2022.108429.
57 K. A. Nxumalo, O. A. Fawole and A. O. Aremu, Development of Chitosan-Based Active Films with Medicinal Plant Extracts for Potential Food Packaging Applications, *Processes*, 2023, **12**(1), 23, DOI: 10.3390/pr12010023.
58 S. Farris, L. Introzzi, P. Biagioni, T. Holz, A. Schiraldi and L. Piergiovanni, Wetting of Biopolymer Coatings: Contact Angle Kinetics and Image Analysis Investigation, *Langmuir*, 2011, **27**(12), 7563–7574, DOI: 10.1021/la2017006.
59 A. A. Shamsuri and S. N. A. M. Jamil, Functional Properties of Biopolymer-Based Films Modified with Surfactants: A Brief Review, *Processes*, 2020, **8**(9), 1039, DOI: 10.3390/pr8091039.
60 B. N. Singh, W. R. Thoden and J. Wahl, Acebutolol: A Review of its Pharmacology, Pharmacokinetics, Clinical Uses, and Adverse Effects, *Pharmacotherapy*, 1986, **6**(2), 45–61, DOI: 10.1002/j.1875-9114.1986.tb03451.x.
61 B. A. Khan, A. Khan, M. K. Khan and V. A. Braga, Preparation and properties of High sheared Poly(Vinyl Alcohol)/Chitosan blended Hydrogels films with Lawsonia inermis extract as wound dressing, *J. Drug Delivery Sci. Technol.*, 2021, **61**, 102227, DOI: 10.1016/j.jddst.2020.102227.

62 P. B. Franco, L. A. De Almeida, R. F. C. Marques, M. A. Da Silva and M. G. N. Campos, Chitosan Associated with the Extract of Unripe Banana Peel for Potential Wound Dressing Application, *Int. J. Polym. Sci.*, 2017, **2017**(1), 9761047, DOI: 10.1155/2017/9761047.

63 C. Y. Chin, J. Jalil, P. Y. Ng and S. F. Ng, Development and formulation of Moringa oleifera standardised leaf extract film dressing for wound healing application, *J. Ethnopharmacol.*, 2018, **212**, 188–199, DOI: 10.1016/j.jep.2017.10.016.

64 Q. Yuan, J. Shah, S. Hein and R. D. K. Misra, Controlled and extended drug release behavior of chitosan-based nanoparticle carrier, *Acta Biomater.*, 2010, **6**(3), 1140–1148, DOI: 10.1016/j.actbio.2009.08.027.

65 F. Ordikhani and A. Simchi, Long-term antibiotic delivery by chitosan-based composite coatings with bone regenerative potential, *Appl. Surf. Sci.*, 2014, **317**, 56–66, DOI: 10.1016/j.apsusc.2014.07.197.

66 W. Huang, C. P. Tsui, C. Y. Tang and L. Gu, Effects of Compositional Tailoring on Drug Delivery Behaviours of Silica Xerogel/Polymer Core-shell Composite Nanoparticles, *Sci. Rep.*, 2018, **8**(1), 1–13, DOI: 10.1038/s41598-018-31070-9.

67 F. Cui, *et al.*, Nanoparticles incorporated in bilaminated films: A smart drug delivery system for oral formulations, *Biomacromolecules*, 2007, **8**(9), 2845–2850, DOI: 10.1021/bm070339e.

68 M. V. S. Varma, A. M. Kaushal, A. Garg and S. Garg, Factors affecting mechanism and kinetics of drug release from matrix-based oral controlled drug delivery systems, *Am. J. Drug Delivery*, 2004, **2**(1), 43–57, DOI: 10.2165/00137696-200402010-00003.

69 D. Samaha, R. Shehayeb and S. Kyriacos, Modeling and comparison of dissolution profiles of diltiazem modified-release formulations, *Dissolution Technol.*, 2009, **16**(2), 41–46, DOI: 10.14227/DT160209P41.

70 A. Craciun, L. Mititelu Tartau, M. Pinteala and L. Marin, Nitrosalicyl-imine-chitosan hydrogels based drug delivery systems for long term sustained release in local therapy, *J. Colloid Interface Sci.*, 2019, **536**, 196–207, DOI: 10.1016/j.jcis.2018.10.048.

71 N. V. Mulye and S. J. Turco, An Examination of Assumptions Underlying the First-Order Kinetic Model for Release of Water-Soluble Drugs from Dicalcium Phosphate Dihydrate Matrices, *Drug Dev. Ind. Pharm.*, 1996, **22**(7), 673–679.

72 R. W. Korsmeyer, R. Gurny, E. Doelker, P. Buri and N. A. Peppas, Mechanisms of solute release from porous hydrophilic polymers, *Int. J. Pharm.*, 1983, **15**(1), 25–35, DOI: 10.1016/0378-5173(83)90064-9.

73 J. Siepmann and N. A. Peppas, Higuchi equation: Derivation, applications, use and misuse, *Int. J. Pharm.*, 2011, **418**(1), 6–12, DOI: 10.1016/j.ijpharm.2011.03.051.

74 J. Chalitangkoon, A. Ronte, T. Sintoppun, N. Manapradit and P. Monvisade, Dual Cross-Linked Chitosan-Based Films with pH-Sensitive Coloration and Drug Release Kinetics for Smart Wound Dressings, *ACS Omega*, 2025, **10**(8), 7770–7782, DOI: 10.1021/acsomega.4c08089.

75 T. N. da Silva, F. Reynaud, P. H. d. S. Picciani, K. G. de Holanda e Silva and T. N. Barradas, Chitosan-based films containing nanoemulsions of methyl salicylate: Formulation development, physical-chemical and in vitro drug release characterization, *Int. J. Biol. Macromol.*, 2020, **164**, 2558–2568, DOI: 10.1016/j.ijbiomac.2020.08.117.

76 A. Craciun, L. Mititelu Tartau, M. Pinteala and L. Marin, Nitrosalicyl-imine-chitosan hydrogels based drug delivery systems for long term sustained release in local therapy, *J. Colloid Interface Sci.*, 2019, **536**, 196–207, DOI: 10.1016/j.jcis.2018.10.048.

77 M. Sakthivel, D. S. Franklin, S. Sudarsan, G. Chitra and S. Guhanathan, Investigation on pH-switchable (itaconic acid/ethylene glycol/acrylic acid) based polymeric biocompatible hydrogel, *RSC Adv.*, 2016, **6**(108), 106821–106831, DOI: 10.1039/c6ra21043k.

78 O. J. D'souza, J. P. Pinto, A. K. Shettar, S. S. Narasagoudr, S. P. Masti and R. B. Chougale, Biofunctionalization of chitosan/gelatin composite films reinforced Phyllanthus niruri extract for wound healing application, *Surf. Interfaces*, 2023, **43**, 103567.

79 T. J. Silhavy, D. Kahne and S. Walker, The bacterial cell envelope, *Cold Spring Harbor Perspect. Biol.*, 2010, **2**(5), a000414, DOI: 10.1101/cshperspect.a000414.

80 S. G. G. Aziz and H. Almasi, Physical characteristics, release properties, and antioxidant and antimicrobial activities of whey protein isolate films incorporated with thyme (Thymus vulgaris L.) extract-loaded Nanoliposomes, *Food Bioprocess Technol.*, 2018, **11**(8), 1552–1565, DOI: 10.1007/s11947-018-2121-6.

81 J. H. Lee, *et al.*, Drug-Loaded Biocompatible Chitosan Polymeric Films with Both Stretchability and Controlled Release for Drug Delivery, *ACS Omega*, 2023, **8**(1), 1282–1290, DOI: 10.1021/acsomega.2c06719.